A One-Dimensional Entraining/Detraining Plume Model and Its Application in Convective Parameterization

JOHN S. KAIN AND J. MICHAEL FRITSCH

Department of Meteorology, The Pennsylvania State University, University Park, Pennsylvania

(Manuscript received 1 February 1990, in final form 18 June 1990)

ABSTRACT

A new one-dimensional cloud model, specifically designed for application in mesoscale convective parameterization schemes (CPSs), is introduced. The model is unique in its representation of environmental entrainment and updraft detrainment rates. In particular, the *two-way* exchange of mass between clouds and their environment is modulated at each vertical level by a buoyancy sorting mechanism at the interface of clear and cloudy air. The new entrainment/detrainment scheme allows vertical profiles of both updraft moisture detrainment and updraft vertical mass flux to vary in a physically realistic way as a function of the cloud-scale environment. These performance characteristics allow the parameterized vertical distribution of convective heating and drying to be much more responsive to environmental conditions than is possible with a traditional one-dimensional entraining plume model.

The sensitivities of the new model to variations in environmental convective available potential energy and vertical moisture distribution in idealized convective environments are demonstrated and its sensitivities to several key control parameters are examined. Finally, the performance of the new model in the Fritsch–Chappell CPS is evaluated. Parameterized heating and drying profiles are elucidated as they relate to the convective environment and to the type of cloud model used in the CPS.

1. Introduction

Moist convective processes in the atmosphere occur almost exclusively on spatial scales smaller than those explicitly resolved by numerical weather prediction models. Consequently, in order to include the effects of convection on numerical weather predictions, the timing, location, and intensity of cumulus convection, as well as the nature of its interactions with the larger scale, must be implicitly inferred from resolvable scale variables; i.e., convection must be parametrically included. Cho (1975) and Frank (1983) discuss the various assumptions utilized to parameterize the effects of moist convection in numerical models.

The primary task of convective parameterization schemes (CPSs) is to estimate the rate of subgrid scale convective precipitation, concomitant latent heat release, and the redistribution of heat, moisture and momentum in the vertical. The manner in which these parameters can be linked to the resolvable scale is highly dependent on the horizontal resolution of a numerical model. For example, CPSs designed for use in numerical models with horizontal grid spacing greater than ~50 km must account not only for the effects of individual convective clouds, but also for the meso-β scale motions induced by the clouds, which are still subgrid scale (Frank 1983). Convective parameterization schemes of this type usually rely on statistical correlations between large scale heating and drying rates and some variables(s) that are readily discernible in a numerical model. For example, Kuo-type schemes (i.e., Kuo 1974; Anthes 1977) relate convective heating to moisture convergence in a column and Arakawa and Schubert's (1974) scheme assumes the existence of a state of quasi-equilibrium between the rate at which the large scale destabilizes the atmosphere and the rate of stabilization by an ensemble of convective clouds. As the horizontal resolution of numerical models approaches the scale of individual convective clouds, however, the mesoscale response to convection becomes a resolvable component of the flow and the relationships between resolvable and parameterized scales can become quite different. Observations suggest that the magnitude of convective heating and drying effects on scales less than ~50 km is much more strongly correlated with local convective available potential energy (CAPE) than with the large-scale rate of destabilization or moisture convergence (Fritsch et al. 1976; Kreitzberg and Perkey 1976).

Furthermore, the assumptions used to parameterize the *vertical distribution* of convective heating and drying on the larger scales become questionable as model resolution is increased and more of the stratiform component of precipitation associated with con-

Corresponding author address: Dr. John S. Kain, Department of Meteorology, The Pennsylvania State University, 503 Walker Building, University Park, PA 16802.

vective systems is explicitly resolved. In particular, on smaller scales the vertical distributions of convective heating and drying become much more strongly linked to individual convective clouds. Since numerous numerical modeling and diagnostic studies have shown that the environmental response to convective heating is extremely sensitive to its vertical distribution (e.g., Gyakum 1983; Hack and Schubert 1986; Fritsch 1986; Kuo and Reed 1988), it seems especially important for CPSs that operate on this scale to enhance their sensitivity to those interactions between individual clouds and their environment which most profoundly affect heating and drying by individual clouds.

Computational constraints limit the degree of sophistication of cloud models used in CPSs, so most schemes utilize simple one-dimensional entraining plume (ODEP) models to represent the thermodynamic and mass flux characteristics of individual clouds. As grid-scale resolution in numerical models approaches the mesoγ scale, convection within each grid element can be characterized by a single type of cloud (Fritsch and Chappell 1980), so that subgrid scale convective processes are typically represented by an ODEP and its associated downdraft. It can be shown (e.g., Frank and Cohen 1985) that the parameterized heating rate throughout most of the depth of the cloud is proportional, on this scale, to the product of the net convective draft (updraft plus downdraft) vertical mass flux and the ambient static stability. Yet, a simple ODEP constrains the mass flux profile by imposing a fixed rate of entrainment, or rate of increase of mass flux, with height. Several investigators have introduced lateral detrainment into ODEP models (i.e., Johnson 1977; Lord 1982; Frank and Cohen 1985), but by restricting the detrainment rate to a constant fraction of the entrainment rate, they have similarly constrained the updraft mass flux profile. A more general version of the ODEP is introduced that allows both entrainment and detrainment to vary in a physically realistic way as a function of the buoyancy characteristics of individual updraft subparcels (see Raymond and Blyth 1986). In this manner, the mass flux in individual updrafts, and hence the parameterized vertical distributions of convective heating and moistening, vary as a function of the cloud-scale environment to enhance the performance of a simple ODEP.

2. A one-dimensional entraining/detraining plume model

Recent observations suggest that most of the mixing between clouds and their environments occurs very near the periphery of clouds in a distinctly nonhomogeneous manner (e.g., Rogers et al. 1985; Jensen and Blyth 1988; Paluch and Baumgardner 1989). These observations indicate that turbulent eddies continuously generate mixtures containing various proportions of clear and cloudy air, implying that the buoyancies of individual cloud subparcels can be quite different from the mean buoyancy of the cloud as a whole (Paluch and Knight 1984; Gardiner and Rogers 1987; Blyth et al. 1988). For example, Fig. 1 evinces the range of subparcel buoyancies that can be expected when an updraft mixes with its environment in random proportions. This figure shows a typical distribution of the virtual temperature difference between mixtures of updraft and environmental air and the unmodified environment. Virtual temperature is estimated by $T_v = T(1 + 0.61r - r_l)$, where r and r_l are the water vapor and liquid mixing ratios, respectively. For the conditions represented in this figure, and assuming thermodynamic equilibrium in individual subparcels, any mixture comprised of about 50% or more environmental air is negatively buoyant with respect to the environment. Conversely, those mixtures containing less than about 50% environmental air remain positively buoyant.

The above observations and this characteristic distribution of temperature as a function of mixing proportion inspire the concept of a new entrainment/detrainment scheme. In the new cloud model, which is aptly called a one-dimensional entraining/detraining plume (ODEDP) model, it is assumed that any mixture that becomes negatively buoyant detrains from the cloud while those mixtures that remain positively buoyant entrain into the cloud. By evaluating this mixing process and updating the mean thermodynamic characteristics of the cloud at regular vertical intervals, the scheme allows the thermodynamic characteristics

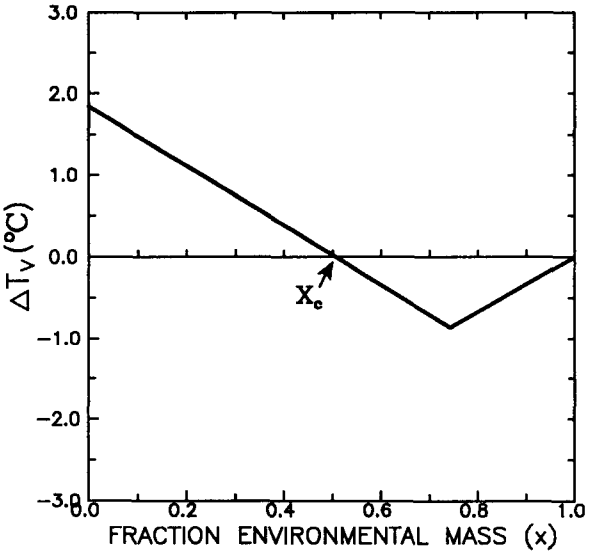

FIG. 1. Plot of typical virtual temperature differences between updraft–environment mixtures and that of the unmixed environment as a function of the fraction of environmental mass in the mixtures. This distribution is derived for an ambient pressure of 600 mb assuming an environmental temperature of 273 K and relative humidity of 70%, updraft temperature of 275 K (saturated) and updraft liquid water mixing ratio of 2 g kg^{-1}.

of the mixing process to modulate the *two-way* exchange of mass between convective clouds and the environments through which they rise.

a. The rate of environmental inflow

The first step in implementing this concept is to estimate the rate at which environmental air mixes with cloudy air. This mixing rate represents an upper bound on the entrainment rate. Typically, however, some of the mass that initially mixes into the cloud combines with updraft air to form negatively buoyant mixtures that presumably will never penetrate far enough to dilute the mean properties of the updraft or contribute to its vertical mass flux. The traditional formulation for entrainment rate, that is, the fractional increase in cloud-mass flux per unit height is inversely proportional to updraft radius (see e.g., Turner 1962; Simpson and Wiggert 1969; Kreitzberg and Perkey 1976) is used as a basis for prescribing the inflow rate. However, this formulation is modified in two ways. First, following Frank and Cohen (1985), the incremental inflow rate is expressed as a function of pressure instead of height, so that it is mass weighted. Second, a linear approximation to the original formulation is used so that the rate of inflow is constant with respect to decreasing pressure. Specifically, the rate, δM_e (units of kg s^{-1}), at which environmental air mixes into an updraft over a pressure interval δp (Pascals) is expressed as

$$\delta M_e = M_{u0}(-0.03\delta p/R), \tag{1}$$

where R and M_{u0} are the updraft radius and mass flux (units of m and kg s^{-1}), at cloud base, and 0.03 is a constant of proportionality (units of m Pa^{-1}) comparable to the dimensionless value of 0.2 derived for z-coordinates (Simpson 1983). Equation (1) dictates, for example, that an entraining plume with an initial radius of 1500 m and no detrainment would double its mass flux after ascending 500 mb.

b. Estimation of net entrainment and detrainment rates

Equation (1) provides an estimate of the rate at which environmental air flows into the turbulent mixing region at the periphery of an updraft, δM_e. It follows that the updraft mass with which this air initially mixes must become available at a corresponding rate, δM_u. Accordingly, it is assumed that the total rate at which mass enters the transition region between clear and cloudy air is given by $\delta M_t = \delta M_e + \delta M_u$.

The next step is to quantitatively partition mass in this transition region of the cloud into entraining and detraining components. To accomplish this, a means of estimating the rate at which ensembles of both negatively and positively buoyant subparcels are generated is needed. A functional probability distribution is utilized to characterize the turbulent generation of mixed subparcels. There is a dearth of observational evidence to suggest the form that this distribution might take, so the sensitivity of our entrainment/detrainment scheme to a number of hypothetical functions has been evaluated. These sensitivities will be discussed after quantifying a distribution that is particularly appealing from an intuitive perspective.

Suppose that turbulent mixing processes show some propensity to mix updraft and environmental air masses in equal portions and that the relative frequency distribution of subparcel mixtures may be reasonably estimated by a Gaussian-type distribution. Specifically, we propose a functional distribution of the form

$$f(x) = A[e^{-(x-m)^2/2\sigma^2} - k], \tag{2}$$

where x is the fraction of environmental air in mixed subparcels, m is the mean of the distribution (in this case 0.5), and σ is the standard deviation of the distribution. We set $\sigma = 1/6$ to encompass ± 3 standard deviations between the truncation points, $x = 0$ and $x = 1$. We include the constant k so that the modified function goes to zero at these points; i.e., $k = e^{-4.5}$. The constant A is defined such that

$$\int_0^1 f(x)dx = 1. \tag{3}$$

In close approximation to the standard Gaussian distribution, $A = (0.97\sigma\sqrt{2\pi})^{-1}$.

Equation (2) gives a specification of the relative rates at which various mixtures are generated, but this application requires an expression in terms of mass rather than number. This conversion requires an assumption relating the total mass in individual mixed subparcels to their mixing proportion. For simplicity, it is assumed that subparcel size is independent of mixing proportion. This assumption allows the total mass distribution to be obtained by simply multiplying the frequency distribution by δM_t, i.e.,

$$\delta M_e + \delta M_u = \delta M_t \int_0^1 f(x)dx. \tag{4}$$

It follows that the individual components of this distribution must be given by

$$\delta M_e = \delta M_t \int_0^1 xf(x)dx \tag{5}$$

and

$$\delta M_u = \delta M_t \int_0^1 (1-x)f(x)dx, \tag{6}$$

where $1-x$ is the mass fraction of updraft mass in the mixed subparcels. The integrand in (5) represents the distribution of environmental mass in mixed subparcels [$E(x)$ in Fig. 2], while the integrand in (6) denotes the analogous distribution for updraft mass [$U(x)$ in Fig. 2]. Since this total mass distribution is symmetric about $x = 0.5$, the integrated areas under $E(x)$ and $U(x)$ are equal; i.e., $\delta M_e = \delta M_u$.

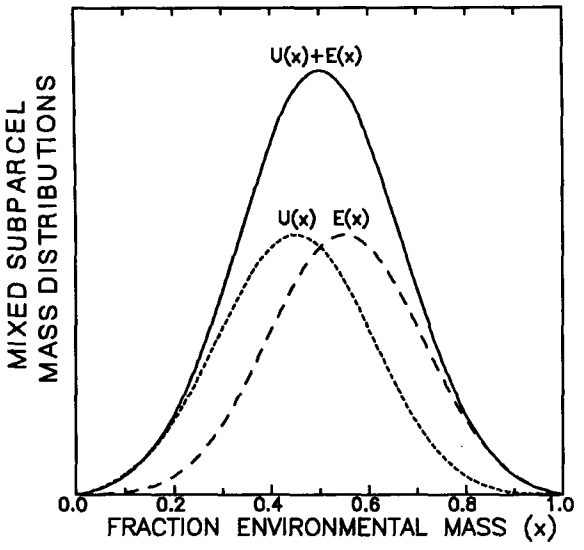

FIG. 2. Hypothetical distribution of environmental mass, $E(x)$; updraft mass, $U(x)$; and total mass, $E(x) + U(x)$, in mixed updraft subparcels as a function of the fraction of environmental air in individual mixed subparcels. The total mass distribution is based on the Gaussian distribution function.

Given these hypothetical distributions of mass in mixed subparcels, the total rate at which both updraft and environmental air mix into subparcels that are positively buoyant (which are assumed to be entraining subparcels) and into those that are negatively buoyant (assumed to be detraining) can be determined. Consider, for example, the conditions represented by Fig. 1. It is assumed that this figure characterizes mixing between an updraft and its environment at a given vertical level. If the fractional amount of environmental mass that just yields a neutrally buoyant mixture is labeled as x_c (in this case $x_c \approx 0.5$), the net environmental entrainment rate at this level, M_{ee}, is given by

$$M_{ee} = \delta M_t \int_0^{x_c} x f(x) dx, \tag{7}$$

and the updraft detrainment rate, M_{ud}, is determined from

$$M_{ud} = \delta M_t \int_{x_c}^{1} (1-x) f(x) dx. \tag{8}$$

c. *Extension of an entraining plume model*

In the ODEDP, this entrainment/detrainment concept is implemented by computing the net exchange of mass at regularly spaced pressure levels and by assuming homogeneous mixing of the entrained air with the bulk of the updraft mass between vertical levels. The thermodynamic characteristics of the updraft, environment, and mixed regions are computed assuming conservation of equivalent potential temperature (θ_e) and total water substance (i.e., the sum of water vapor r, liquid water r_l, and ice r_i, mixing ratios). As described below, it is assumed that cloud condensate is continuously removed from the updraft by precipitation processes.

1) CONVERSION OF CONDENSATE TO PRECIPITATION

Following Ogura and Cho (1973), allowed condensate (without differentiating between liquid and solid forms) is to be removed from the updraft such that the amount lost, δr_c, in a given layer of depth δz is given by

$$\delta r_c = r_{co}(1 - e^{-c_1 \delta z / w}), \tag{9}$$

where w is the mean vertical velocity in the layer, r_{c0} is the concentration of condensate at the bottom of the layer plus one-half the degree of supersaturation at the top, and c_1 is a rate constant. Typical profiles of updraft condensate concentration given the ODEDP with this conversion scheme and c_1 ranging from 0.005–0.02 s^{-1} are shown in Fig. 3. These curves are derived from a convective environment with ambient convective available potential energy (CAPE) on the order of 1000 $m^2 s^{-2}$. Since the precipitation conversion rate is an inverse function of w, the maximum concentration of condensate varies, for example, from about 0.5 to 3.0 g kg^{-1} as the CAPE varies from about 100 to 4000 $m^2 s^{-2}$ when $c_1 = 0.01$ s^{-1} is used. These values seem reasonably consistent with a wide range of observational and numerical modeling results (Hallet et al. 1978; Heymsfield and Musil 1982; Hauser and Ameyenc 1986; Waldvogel et al. 1987; Orville 1987, personal communication; Weisman 1988, per-

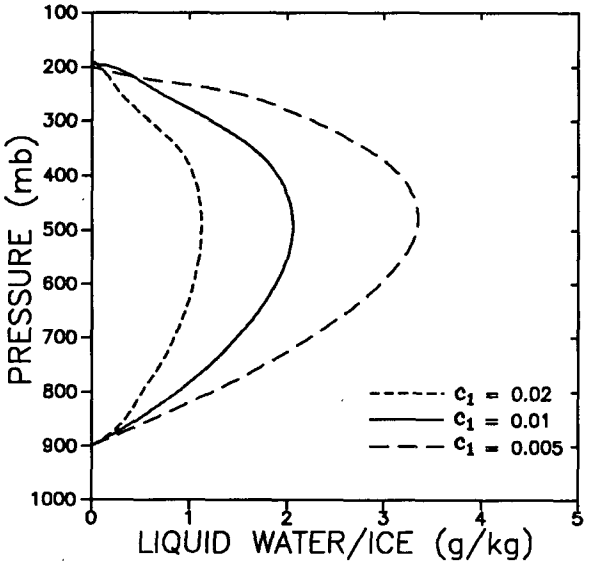

FIG. 3. Typical profiles of parameterized updraft liquid water/ice concentrations predicted by the ODEDP as a function of the condensate conversion rate, c_1.

sonal communication; Weissbluth and Cotton 1988, personal communication; Jorgensen and LeMone 1989). Accordingly, $c_1 = 0.01\ s^{-1}$ is used as a default value.

2) CLOUD GLACIATION

Glaciation processes are parameterized in the ODEDP by assuming a linear transition from θ_e with respect to liquid water to θ_e with respect to ice from 268 K to 248 K. Similar approaches have been taken by Lord et al. (1984) and Tao et al. (1989). A hybrid value of θ_e is used during the transition. Specifically, θ_e is expressed as

$$\theta_e = \theta \exp[1.0723(10)^{-3}(1 + 0.81r)Lr/T], \quad (10)$$

following Bolton (1980). During the transition from liquid-water saturation thermodynamics to ice saturation thermodynamics we assume that

$$L = (1 - \nu)L_v + \nu L_s \quad (11)$$

and

$$r = (1 - \nu)r_{sl} + \nu r_{si}, \quad (12)$$

where L_v and L_s are the magnitudes of latent heating for the vaporization and sublimation processes, respectively; r_{sl} and r_{si} are saturation water vapor pressure over liquid water and over ice, respectively; and ν is a measure of the degree of glaciation.

The freezing of condensate takes place in a similar manner. At each vertical level within the specified temperature range, a fraction of the liquid condensate, consistent with the linear transition, is converted to ice. The magnitude of the latent heat release at any level due to the glaciation process is a function of the combined influence of the freezing of liquid water and any evaporation/sublimation required to maintain saturation at the new temperature and hybrid saturation mixing ratio.

3. Sensitivities of the new cloud model

The ODEDP is designed to enhance the sensitivity of an entraining plume model to cloud-scale thermodynamic conditions. In this section, idealized environmental soundings are utilized to evaluate the efficacy of the new model and discuss the sensitivity of the model to some key control parameters. As we will discuss later, the vertical profile of updraft mass flux has a profound influence on the vertical profiles of convective heating and moistening predicted by a CPS. Hence, the model predicted updraft mass flux profile is used to gauge its performance.

a. Sensitivity to environmental moisture profile and CAPE

Consider the idealized environmental soundings shown in Figs. 4a,b. The soundings are identical below

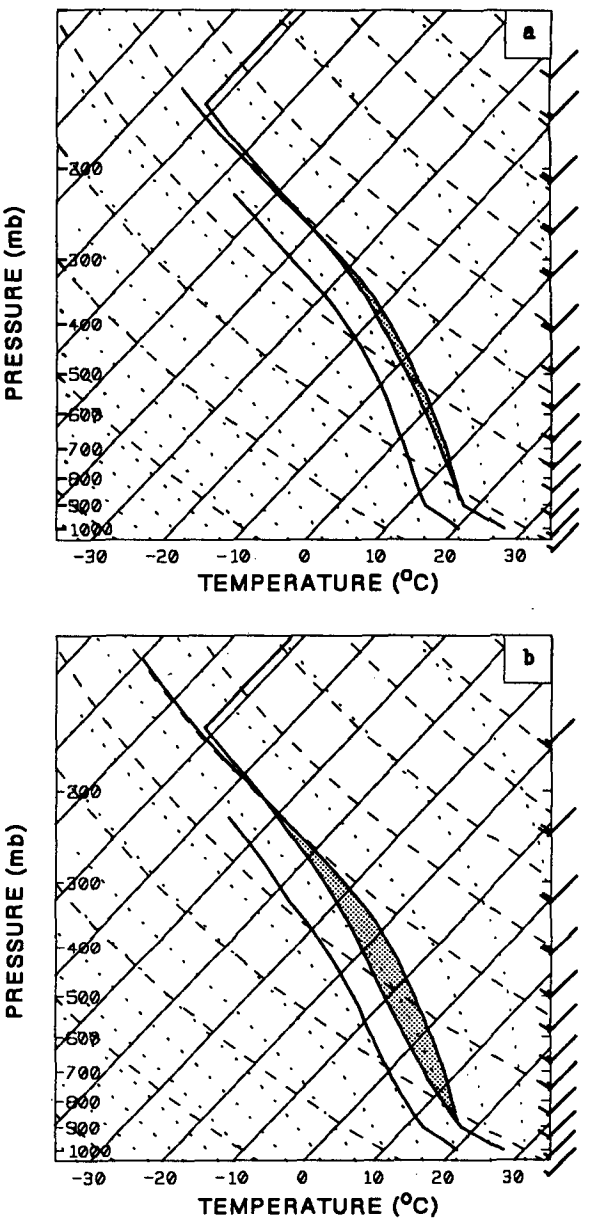

FIG. 4. Idealized environmental soundings used for ODEDP sensitivity tests. (a) Low CAPE environment with a lifted index of −2. (b) Higher CAPE environment with a lifted index of −5. Note that the indicated updraft paths represent undilute moist adiabatic ascent. Full wind barb represents 5 m s^{-1} wind speed, dashed lines are dry adiabats, and dotted lines are moist adiabats.

925 mb so that simulated updraft parcels begin with the same thermodynamic characteristics. The updraft paths predicted by pseudoadiabatic ascent are used to enclose the positive areas on the diagrams (stippled regions). Figure 4a represents a marginally unstable environment with the maximum temperature difference between the environment and a moist adiabat through the lifting condensation level (LCL) being 2°K. Figure 4b evinces an environment with consid-

erably more CAPE and a maximum undilute updraft temperature perturbation of 5°K. In both cases, the humidity profile shown represents a constant relative humidity of 70% between the LCL and the tropopause. The relative humidity is varied from 50% to 90% for each of these temperature profiles to demonstrate the model sensitivities.

Figure 5a shows updraft mass flux profiles (normalized by the mass flux at cloud base) for the lower CAPE environment. The profiles vary considerably. In general, the potential for evaporative cooling due to mixing of environmental air into the updrafts increases as relative humidity decreases, so that the model predicts that an updraft rising through the driest environment detrains most of its mass well below cloud top. Conversely, a very moist environment (RH = 90%) renders most mixtures of updraft and environmental air positively buoyant with respect to the environment so that entrainment dominates the turbulent exchange of mass across the boundaries of the updraft in our model. The contrasting character of the clouds implied by these profiles would have a significant impact on heating and moistening profiles predicted by a CPS.

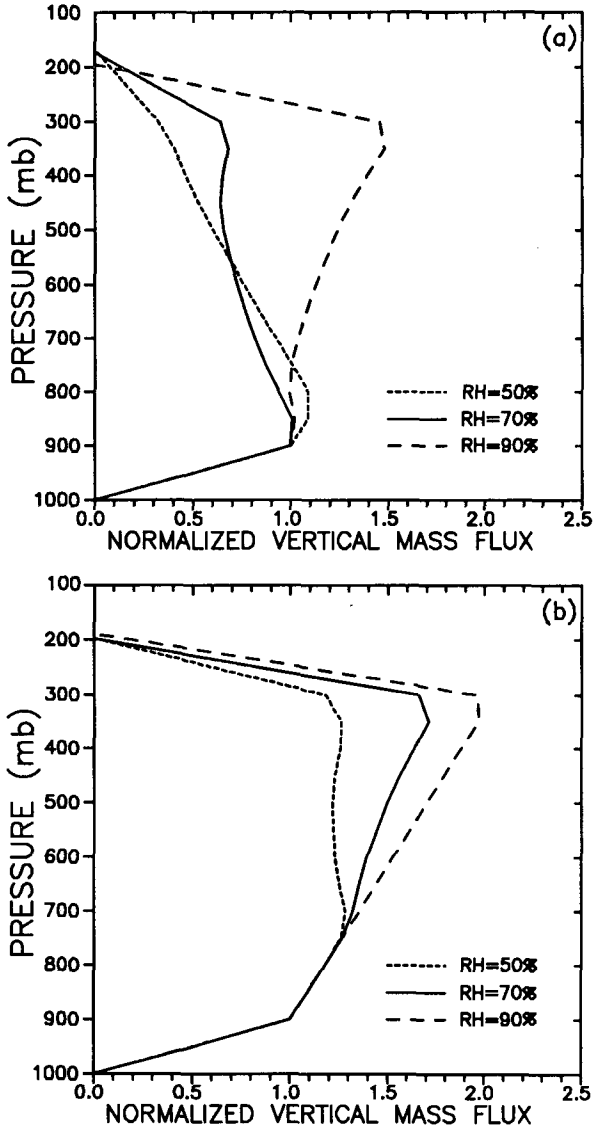

FIG. 5. Sensitivity of ODEDP mass flux profiles to environmental relative humidity for the environmental temperature profiles shown in Fig. 4a and Fig. 4b.

Figure 5b shows corresponding mass flux profiles for the higher CAPE scenario of Fig. 4b. In general, detrainment below cloud top is comparatively suppressed in this environment by the larger updraft temperature perturbations. At lower levels, the liquid-water concentrations are too low for evaporation to cool any mixture of updraft and environmental air below the ambient temperature, resulting in a steady increase in mass flux up to about 750 mb for all three humidity profiles. Above this level, however, the simulated mass flux profiles diverge sharply.

b. Sensitivity to model parameters

1) MIXED SUBPARCEL MASS DISTRIBUTION

A rather arbitrary frequency distribution is imposed for the rate of generation of all mixing proportions and is converted to a mass distribution by assuming that subparcel size is independent of mixing proportion. Observational evidence in this regard is very limited, but recent high spatial resolution observational data suggests that progress towards quantifying and validating parameterized cloud-scale mixing processes. For example, the fine-scale measurements of Paluch and Baumgardner (1989) suggest that smaller subparcels within a cloud may, on average, be more diluted than larger ones.

The sensitivity of the ODEDP to multiple combinations of assumed frequency and subparcel size distributions as a function of mixing proportion has been evaluated. Updraft mass flux profiles predicted by the ODEDP show some sensitivity to variations in the distribution of mass that result from these combinations. For example, as an alternative to the Gaussian-type profile, consider a flat total-mass distribution derived by assuming that subparcels comprised of any proportion of updraft and environmental air are equally likely to be generated and that subparcel size is independent of mixing proportion. This total mass distribution yields the updraft and environmental mass distributions, $E(x)$ and $U(x)$, shown in Fig. 6. If these distributions are substituted into the ODEDP, the environmental thermodynamic profiles of Figs. 4a,b (i.e., RH = 70%) yield the mass flux profiles shown in Fig. 7. These figures suggest that both entrainment and detrainment are relatively suppressed with these alternative distributions. Indeed, it is found that when x_c = 0.5, for example, entrainment and detrainment rates

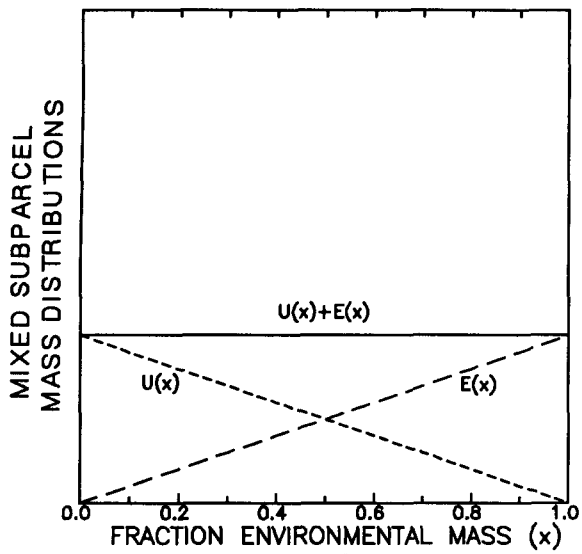

FIG. 6. Hypothetical distributions of environmental mass, $E(x)$; updraft mass, $U(x)$; and total mass, $E(x) + U(x)$, in mixed updraft subparcels as a function of the fraction of environmental air in individual mixed subparcels. The total mass distribution is based on a simple flat distribution function.

are both about 37% of the environmental inflow rate with the Gaussian-type distribution, but only about 25% of the inflow rate with the flat distribution.

These results are consistent with the evaluation of numerous other mixing distribution functions, including skewed distributions in which $\delta M_e \neq \delta M_u$. In general, the magnitude of updraft mass flux may vary considerably, especially at upper levels, as a function of the mixing distribution. It appears, however, that the general form of the mass flux profile and the sign of $\partial M/\partial P$ are primarily dictated by the environmental thermodynamic profile. For the remainder of this study, it was chosen to implement the Gaussian-type mixing distribution only because it represents an intuitively credible hypothesis for what may occur in nature. It is acknowledged, however, that preferred selection of any mixing distribution requires a small leap of faith since it is also intuitive that many environmental factors (e.g., static stability and vertical wind shear) may affect the distribution.

2) RATE OF ENVIRONMENTAL INFLOW

Mass flux profiles generated by the ODEDP are particularly sensitive to the rate of environmental inflow, or cloud size. For example, Figs. 8a,b show ODEDP mass flux profiles for the environmental soundings of Figs. 4a,b (RH = 70%) and for specified cloud radii of 500, 1500, and 2500 m. The profiles vary dramatically, but this sensitivity is not unique to the ODEDP. The uncertainties regarding both the environmental controls on cloud size and the validity of the inverse radius entrainment relationship have presented a chronic challenge for users of one-dimensional entraining plume models of cumulus clouds in a prognostic context (e.g., see Simpson 1971; Kreitzberg and Perkey 1976; Anthes 1977).

There is some evidence to suggest that the cloud size may be related to local mass convergence. For example, cloud-scale numerical modeling results suggest that larger clouds are increasingly suppressed when background mass convergence is artificially reduced (see Tao and Simpson 1984; Krueger 1988). Furthermore, the inverse radius entrainment relationship implies a dependence on cloud dimensions that is not inconsistent with recent observations (Blyth et al. 1988). Frank and Cohen (1985) found sufficient observational evidence from GATE (Global Atmospheric Research Programme Atlantic Tropical Experiment) data to introduce an entrainment relationship based on mesoscale mass convergence. Their CPS, designed for use in mesoscale models, utilizes a plume model with the entrainment rate inversely proportional to the square root of resolvable scale, low-level mass convergence. For a given cloud-base vertical velocity, this relationship is equivalent to a dependence on $1/R$. Their approach has been quite successful and a similar relationship for using the ODEDP within a CPS in a prognostic model may be adapted in future mesoscale modeling studies. For the present study, unless otherwise indicated, the mass inflow rate given by (1) with R = 1500 m is utilized.

3) OTHER PARAMETERS

The sensitivity of the ODEDP to several other parameters, including the value of the precipitation conversion rate, cloud glaciation effects, and model vertical

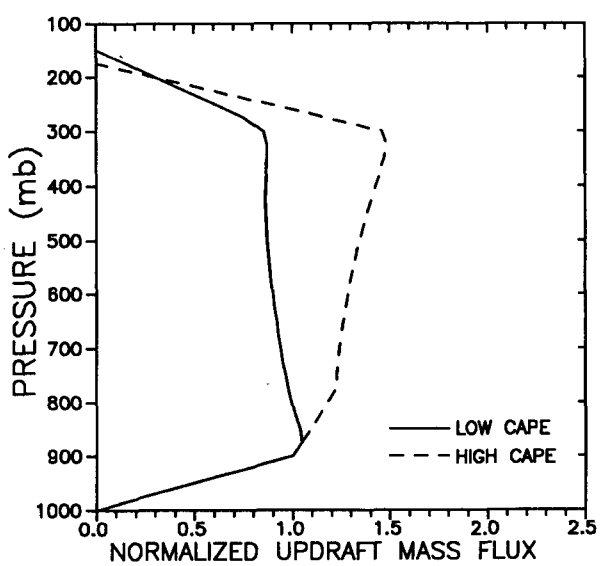

FIG. 7. Mass flux profiles derived from the ODEDP using the mass distribution functions shown in Fig. 6 and the thermodynamic profiles of Figs. 4a (low CAPE) and 4b (high CAPE).

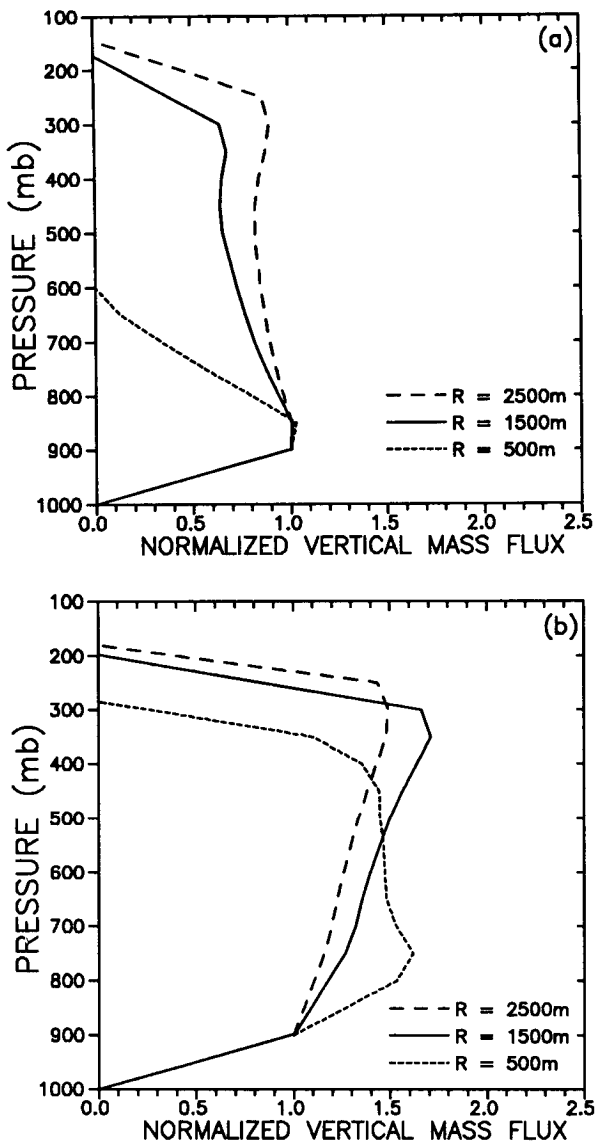

FIG. 8. Sensitivity of ODEDP mass flux profiles to the rate of environmental inflow imposed by specification of the indicated cloud radii, for the environmental soundings shown in Fig. 4a and Fig. 4b.

resolution have also been investigated. The model is generally much less sensitive to these parameters than it is to the assumed mass distribution of mixed parcels and to cloud radius.

4. Performance of the new cloud model in a convective parameterization scheme

The performance of the ODEDP is evaluated in a convective parameterization framework by incorporating it into the Fritsch and Chappell (FC, 1980) CPS. Accommodation of the new cloud model necessitates a number of other minor changes in the scheme, particularly with regard to the liquid-water budget, but the basic closure assumptions of FC remain unchanged. Details of the modifications can be found in Kain (1989).

In the first part of this section, the sensitivity of the modified FC scheme to variations in environmental relative humidity is demonstrated, utilizing the idealized soundings of Figs. 4a,b. Subsequently, real data is used to compare results obtained with the ODEDP to those derived from plume models that use two other types of entrainment/detrainment relationships (all within the modified FC scheme). The first is a simple entraining plume model with no detrainment below cloud top, similar to that used by Arakawa and Schubert (1974), Kreitzberg and Perkey (1976), and Anthes (1977). The second is an entraining/detraining plume with the detrainment rate specified as a constant fraction of the entrainment rate, as used by Johnson (1977), Lord (1982), and Frank and Cohen (1985). In this case, the detrainment rate is set equal to the entrainment rate at all levels below cloud top. In addition, the individual components of the total heating and drying profiles derived are delineated when the ODEDP model is used.

a. Quantification of parameterized effects

Following Ooyama (1971), Yanai et al. (1973), Arakawa and Schubert (1974), Frank and Cohen (1985) and others, the rate of parameterized convective heating at a given vertical level can be approximated in the FC scheme by

$$\left.\frac{\partial \tilde{T}}{\partial t}\right|_{\text{conv}} = \left(\frac{M_u + M_d}{\tilde{\rho}A}\right)\left(\Gamma + \frac{\partial \tilde{T}}{\partial z}\right) + \frac{M_{ud}}{\tilde{\rho}A\delta z} \times (T_u - \tilde{T}) + \frac{M_{dd}}{\tilde{\rho}A\delta z}(T_d - \tilde{T}) - \frac{M_{ud}}{\tilde{\rho}A\delta z}\frac{r_c L}{C_p}, \quad (13)$$

where M_u and M_d are the updraft and downdraft mass fluxes ($M_d < 0$); M_{ud} and M_{dd} are the rates of detrainment from the updraft and downdraft (all in units of kg s^{-1}); Γ is the dry-adiabatic atmospheric lapse rate; T_u, T_d, and $\tilde{T}$ are the updraft, downdraft, and environmental temperatures, respectively; $\tilde{\rho}$ is density of the environment air; r_c is the liquid water and/or ice mixing ratio in the updraft; L is the appropriate magnitude of latent heating per unit mass, and A is the horizontal area represented by a model grid element. The first term in brackets on the right-hand side gives the magnitude of the compensating environmental vertical motions required to offset the convective mass flux. Since the mass flux in convective updrafts is often a factor of two or more greater than in their associated downdrafts (LeMone and Zipser 1980; Knupp and Cotton 1985), the compensating motion is typically in the form of subsidence. Furthermore, since the updraft dominates, it is anticipated that the variations in updraft mass flux as predicted by the ODEDP will have a significant impact on the vertical distribution of parameterized convective heating and drying.

It is worth noting that the magnitude of compensating subsidence tends to increase exponentially with height even when updraft mass flux is constant with height; for example, if constant mass flux with height is assumed, $\tilde{w}(z) \propto \tilde{\rho}(z)^{-1}$, and since $\tilde{\rho}(z) \sim \rho_0 e^{-z/H}$, $\tilde{w} \propto e^{z/H}$. For a given stability profile, parameterized convective heating tends to be skewed towards higher levels relative to the net mass flux profile in this type of CPS.

Equation (13) can be expressed more succinctly as

$$\left.\frac{\partial \tilde{T}}{\partial t}\right|_{\text{conv}} = \underbrace{-\tilde{w}\left(\Gamma + \frac{\partial \tilde{T}}{\partial z}\right)}_{\text{A}} + \underbrace{\frac{M_{ud}}{\tilde{M}}(T_u - \tilde{T})}_{\text{B}} + \underbrace{\frac{M_{dd}}{\tilde{M}}(T_d - \tilde{T})}_{\text{C}} - \underbrace{\frac{M_{ud}}{\tilde{M}}\frac{r_c L}{C_p}}_{\text{D}}, \quad (14)$$

where $\tilde{M}$ is the effective mass of environmental air represented by each model level. The terms on the right-hand side of (14) represent the vertical advection of $\tilde{T}$ by compensating environmental vertical motions (A), the effects of detrainment of updraft (B) and downdraft (C) mass into the environment, and the evaporation/sublimation of detrained condensate in the environment (D).

In a form directly analogous to (14), the parameterized convective drying rate at a given vertical level can be denoted by

$$\left.\frac{\partial \tilde{r}}{\partial t}\right|_{\text{conv}} = -\tilde{w}\frac{\partial \tilde{r}}{\partial z} + \frac{M_{ud}}{\tilde{M}}(r_u - \tilde{r}) + \frac{M_{dd}}{\tilde{M}}(r_d - \tilde{r}) + \frac{M_{ud}}{\tilde{M}} r_c, \quad (15)$$

where r_u, r_d, and $\tilde{r}$ are the updraft, downdraft, and environmental water vapor mixing ratios at a given level; so that terms on the right-hand side once again represent vertical advection, updraft and downdraft detrainment, and evaporation of detrained condensate in the convective environment. Heating and drying rates will both be converted to units of °K day^{-1} [requiring (15) to be multiplied $-L/C_p$].

b. *Sensitivity to environmental moisture profile and CAPE*

Figures 9a,b show parameterized heating profiles generated by the modified FC CPS corresponding to the mass flux profiles in Figs. 5a,b and the environmental temperature profiles in Figs. 4a,b. Clearly, the scheme responds strongly to the ODEDP's sensitivity to environmental relative humidity. Heating profiles from the lower CAPE environment exhibit the same qualitative shape as the mass flux profiles, with the level of maximum heating ranging from cloud base (900 mb) in the driest environment to about 350 mb in the most humid environment.

In the more unstable environment of Fig. 4b, the parameterized convective heating maximizes at about 400 mb regardless of the humidity in the environment. Furthermore, although the modified FC scheme yields the same shape of heating profile for the different humidity environments, the magnitude of total heating varies considerably. In particular, the parameterized

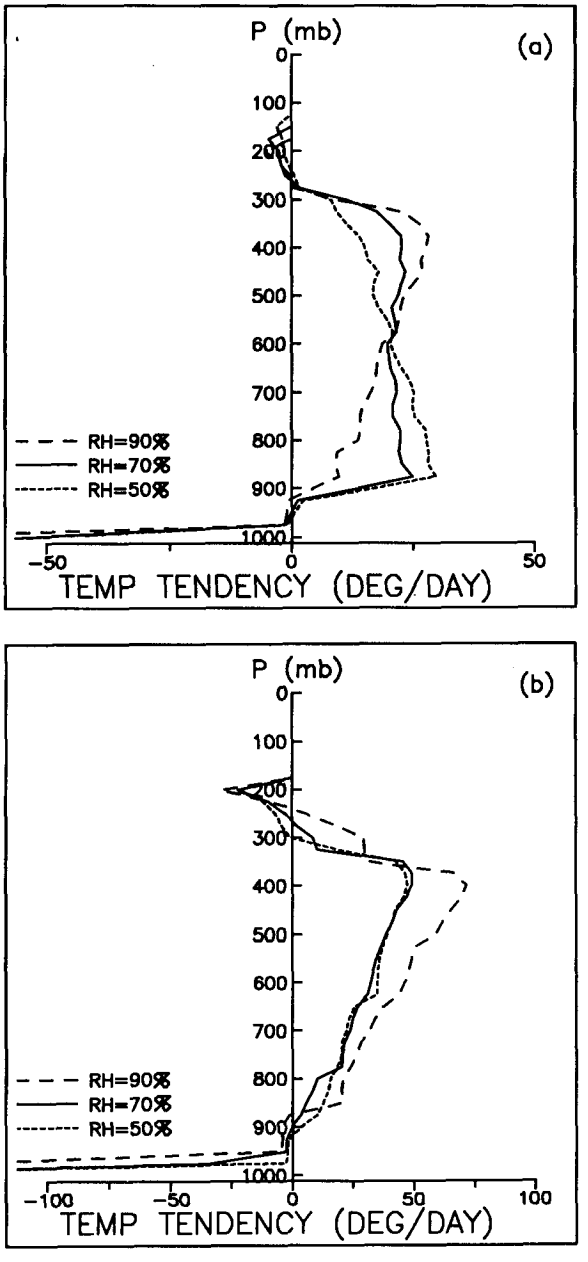

FIG. 9. Parameterized convective heating profiles corresponding to the mass flux profiles in Figs. 5a and 5b, and the environmental thermodynamic profiles of Figs. 4a and 4b, respectively.

vertically integrated heating rate in the moist (90% relative humidity) environment is 44% larger than in the dry (50% relative humidity). The drier environment allows downdrafts to be initiated with lower θ_e air, resulting in a cooler boundary layer outflow and more efficient stabilization of the environment.

c. Sensitivity to cloud-model type

In order to explore the sensitivity of the FC CPS to cloud-model type in different convective environments, two soundings have been selected: the first is representative of the midlatitude severe storm environment of the High Plains, while the second is representative of a maritime tropical environment. In addition to exploring the cloud-model sensitivities, it will be shown that (i) the vertical distribution of convective heating and drying can vary substantially as a function of convective environment and (ii) some of the environmental factors that contribute to making heating profiles so different can be delineated.

1) SEVERE STORM SOUNDING

Figure 10 depicts a selected severe storm environment, where the positive area associated with the updraft path predicted by the ODEDP is stippled and the negative area associated with the downdraft, derived separately in the FC scheme, is cross-hatched. This environment is characterized by very high CAPE (about 3600 $m^2 s^{-2}$), a relatively dry troposphere, especially above 500 mb, a comparatively low tropopause distinguished by a sharp stability gradient, and strong vertical wind shear. (The conditions depicted in Fig. 10 are based on a sounding taken 0000 UTC 3 May 1979 at Oklahoma City, but the original data have been modified to facilitate interpretation and comparison of the parameterized heating and drying profiles of different soundings. In particular, environmental temperature profiles have been smoothed at both the top and bottom of the troposphere and the sounding has been extrapolated from the original surface pressure of 958 mb down to 1000 mb, assuming constant potential temperature and mixing ratio in this layer. As a consequence of these modifications, parameterized cooling rates due to both updraft and downdraft detrainment have been slightly accentuated, but the vertical distribution of heating and drying rates within the cloud layer is not significantly affected.)

Figure 11a shows parameterized convective heating profiles for the ODEDP model (labeled VARIABLE E/D), a simple entraining plume model (ENTRAIN ONLY), and a plume model with the detrainment rate specified as equal to the entrainment rate (DET = ENT); all derived using the modified FC scheme in this environment. The most obvious characteristic of this figure is that there is remarkably little variation in the shape of the heating profile as a function of cloud-model type. All three profiles are dominated by an upper-level heating–cooling couplet.

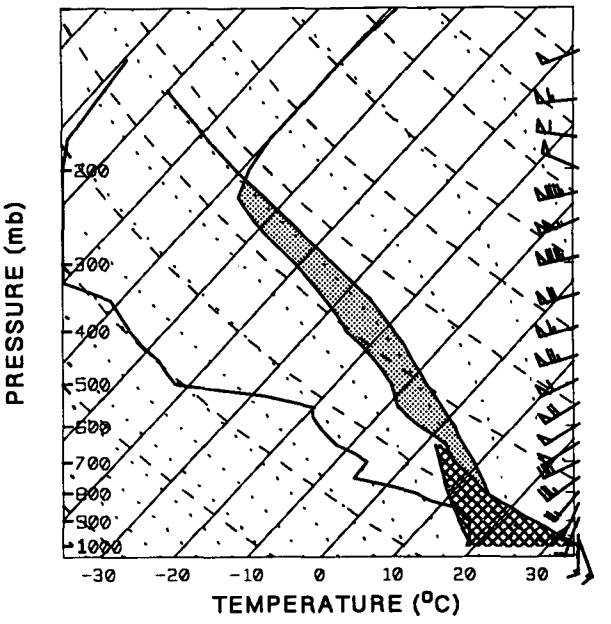

FIG. 10. Severe storm convective environment showing the positive area given by the ODEDP cloud model (stippled) and the downdraft negative area given by the downdraft plume model in the modified FC scheme (cross-hatched). Flag represents 25 m s^{-1} wind speed.

The consistency of this response can be largely explained in terms of the factors that dictate the magnitude of subsidence warming; i.e., the magnitude of subsidence itself coupled with static stability. Figure 12a shows parameterized vertical subsidence profiles as a function of cloud-model type. The ODEDP behaves very much like a simple entraining plume model in this high-CAPE environment so the subsidence profiles associated with these two models (VARIABLE E/D and ENTRAIN ONLY) are nearly homologous. By comparison, the constant mass flux model (DET = ENT) forces stronger subsidence in the lower to middle troposphere and weaker subsidence aloft, consistent with relative heating rates shown in Fig. 11a. The prominence of the upper-level heating maximum overshadows these differences however. Exceptionally strong static stability (Fig. 12b) combines with maximum subsidence rates near cloud top to produce the sharp heating peak. The product of compensating vertical motion and static stability [term A in Eq. (14)], as a function of cloud-model type, is shown in Fig. 12c. Comparison of this profile with the total heating distributions shown in Fig. 11a reveals the dominant contribution of subsidence warming to the total heating throughout most of the cloud layer. Furthermore, note the sensitivity of the heating profiles to variations in static stability. Relative heating maxima are clearly associated with stable layers in the environment.

The impact of updraft and downdraft detrainment effects and evaporational/sublimational cooling [terms B, C, and D, respectively, in (14)] on the total heating rates is strongest below cloud base and near cloud top in this environment. Figure 13a depicts the individual components of the heating for this environment when the ODEDP model is used. The subsidence warming tendency (VERT ADVEC) is considerably weaker than the tendency shown in Fig. 12c because mass detrainment and evaporation effects near cloud top weaken the static stability at this level as the modified FC scheme integrates forward in time over the convective time period (see FC 1980). More specifically, the heating rates shown in Fig. 12c are derived from the initial thermodynamic profile, while the tendencies in Fig. 13a depend on environmental conditions that vary with time as a function of all parameterized cloud scale effects.

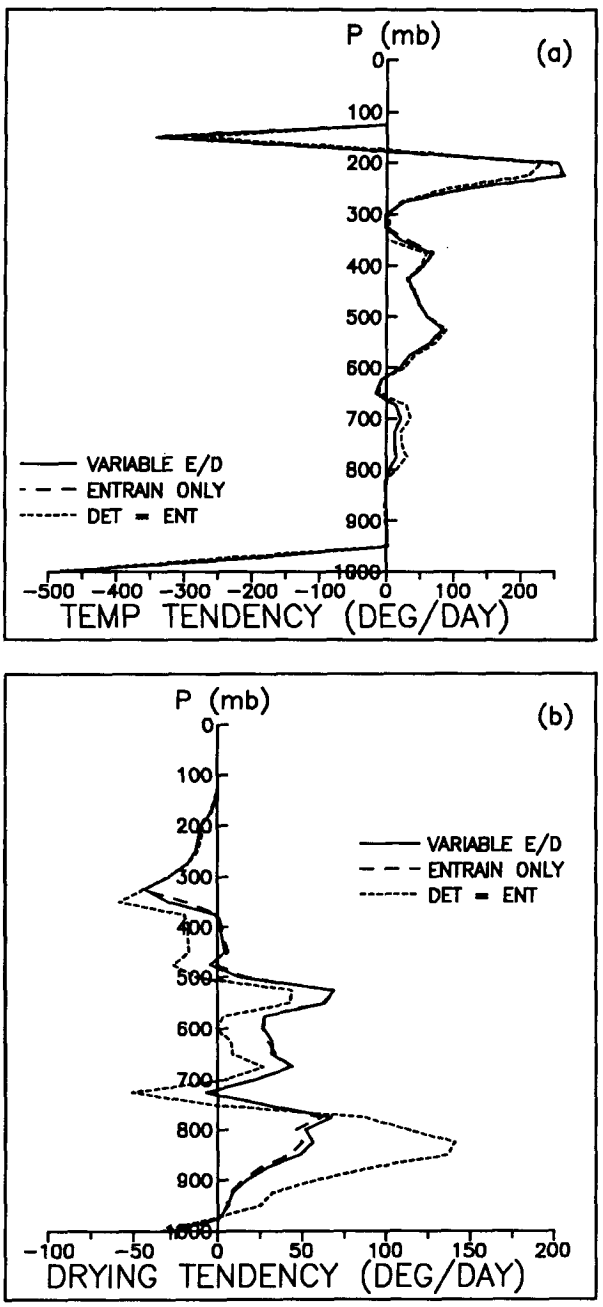

FIG. 11. Parameterized convective heating (a) and drying (b) profiles as a function of cloud-model type for the severe storm environment shown in Fig. 10.

Also, the effects of precipitation melting just below the freezing level are parameterized in the modified FC scheme. The cooling tendency associated with this effect is generally relatively small, consequently it is not represented in (14) or Fig. 13a. However, this effect is to blame for the shallow layer of negative temperature tendency near 650 mb in Fig. 11a. It is also worth noting that the cumulative effects of melting during simulations of mesoscale convective systems using the FC scheme can significantly influence mesoscale circulations (see e.g., Zhang 1989).

Corresponding parameterized convective drying profiles (Fig. 11b) are consistent with the above discussion. The relatively large subsidence rates associated with the constant mass flux model are clearly reflected by much stronger drying tendencies in the lower troposphere. However, this characteristic is confined to the layer between the source layers for updraft air (the lowest two model levels) and the lifting condensation level (LCL). Above the LCL, the detrainment that is prespecified in the constant mass flux model offsets much of the subsidence drying tendency. In contrast, detrainment is limited to cloud top in the simple entraining plume model, and detrainment below cloud top is very limited in this environment with the ODEDP model. Consequently, vertical profiles of parameterized drying tendency derived from the latter two cloud models are principally determined below cloud top by the product of the subsidence rate and the vertical gradient of water vapor mixing ratio [the first term on the RHS of (15)]. This characteristic is shown for the ODEDP model in Fig. 13b. Note that the detrainment curve plotted in this figure (and in Fig. 17b) includes the effects of both detrainment of water vapor from clouds and evaporation of detrained condensate.

2) TROPICAL SOUNDING

Figure 14 shows a tropical environmental sounding representing composite thermodynamic and wind profiles of the initial stages of mesoscale convective systems observed during the GATE study (Frank and McBride 1989). Note the moist boundary layer, the relatively low environmental CAPE (about 1500 m^2 s^{-2}), and the relatively high and gradual transition to the tropopause. In general, the troposphere is quite

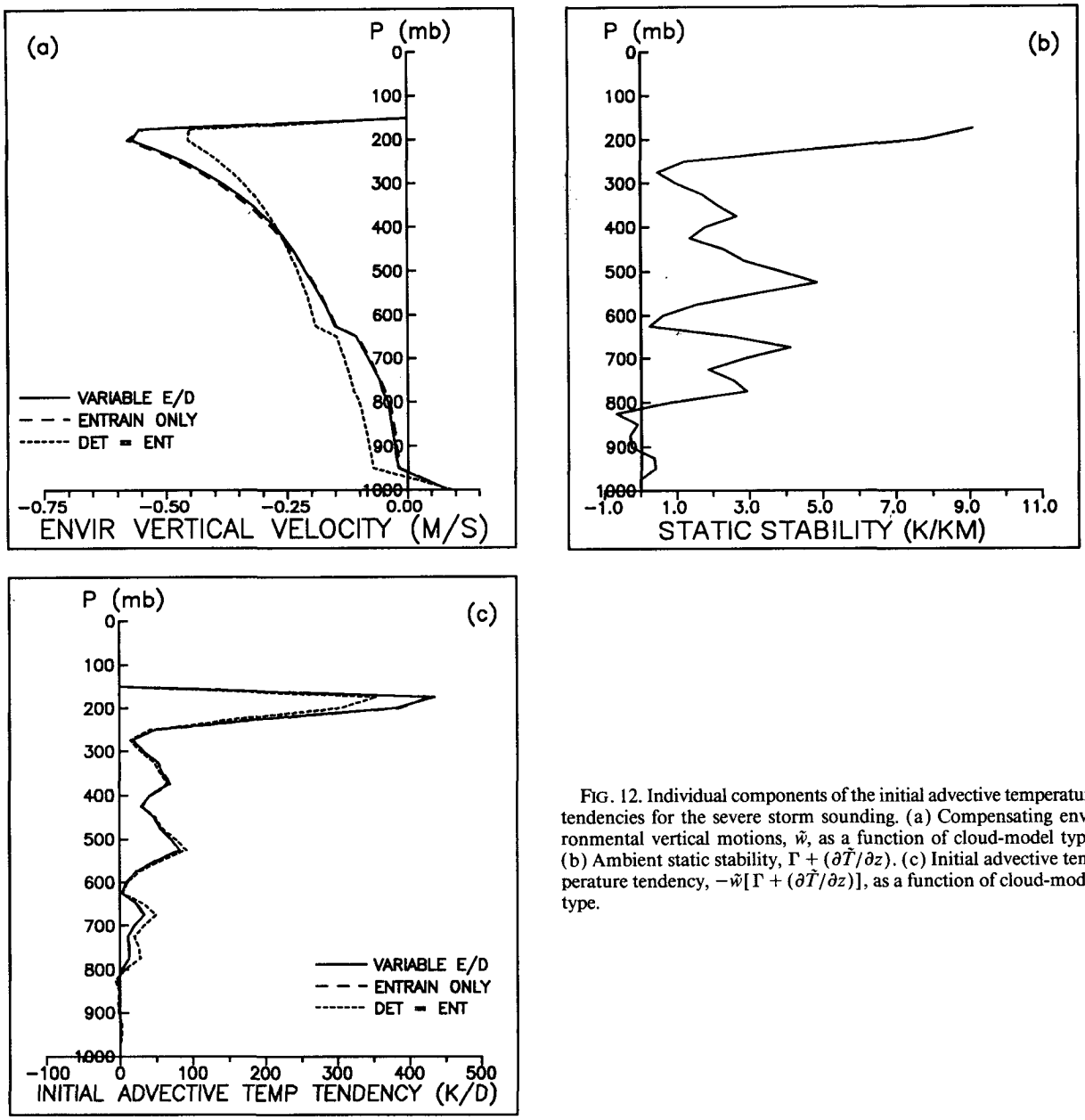

FIG. 12. Individual components of the initial advective temperature tendencies for the severe storm sounding. (a) Compensating environmental vertical motions, $\tilde{w}$, as a function of cloud-model type. (b) Ambient static stability, $\Gamma + (\partial \tilde{T}/\partial z)$. (c) Initial advective temperature tendency, $-\tilde{w}[\Gamma + (\partial \tilde{T}/\partial z)]$, as a function of cloud-model type.

moist, but as noted by Frank and McBride, it may be somewhat anomalously dry by maritime tropical standards.

Parameterized convective heating and drying profiles for this environment, as a function of cloud-model type, are plotted in Figs. 15a,b, respectively. These profiles are derived assuming a cloud radius of 1 km, which is more consistent with the GATE area cloud diameter statistics of LeMone and Zipser (1980) than the previously used value of 1.5 km. With regard to Fig. 15a, note that the parameterized convective heating profile is strongly dependent on cloud model type. The ODEDP focuses most of the heating below 750 mb. In contrast, the other two cloud models tend to concentrate a much larger fraction of the heating in the middle and upper troposphere.

These differences are closely related to the disparate updraft mass flux profiles predicted by the different cloud models. The mass flux profiles are reflected in the corresponding vertical profiles of compensating subsidence, shown in Fig. 16a. Since the subsidence profile associated with the ODEDP is nearly constant with height (implying *decreasing* updraft mass flux with height), the vertical profile of subsidence warming

based on the initial environmental conditions (Fig. 16c) closely follows the static stability profile (Fig. 16b). Because the compensating subsidence maximizes rather sharply near cloud top when the other two cloud models are used, subsidence heating is skewed upward relative to the initial static stability profile.

The individual components of heating associated with the ODEDP (and integrated over the convective time period) are shown in Fig. 17. Subsidence warming dominates the parameterized heating, but is countered

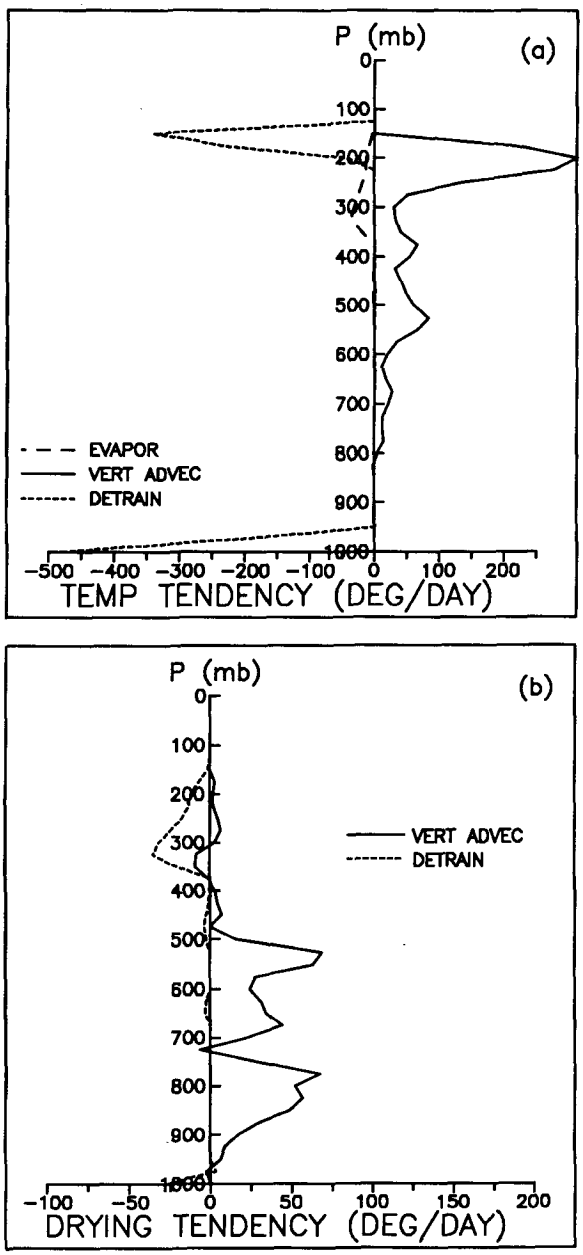

FIG. 13. Individual components of parameterized convective heating (a) and drying (b) for the severe storm sounding when the ODEDP model is used.

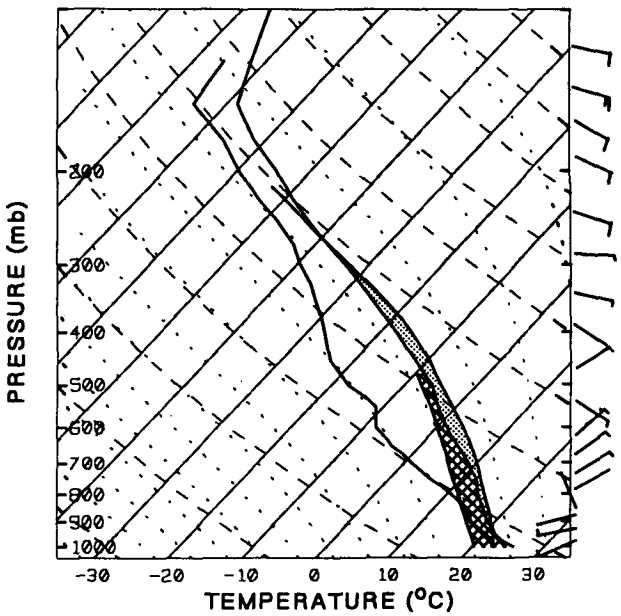

FIG. 14. Tropical (GATE composite) environmental sounding showing the positive area given by the ODEDP cloud model (stippled) and the downdraft negative area given by the downdraft plume model in the modified FC scheme (cross-hatched).

at most levels by evaporational cooling. Lateral detrainment of relatively warm updraft air makes a small positive contribution throughout most of the depth of the cloud. (Mass is not allowed to detrain in the ODEDP unless it is virtually colder than the environment. However, it is more efficient to calculate entrainment and detrainment rates within a cloud model subroutine in the modified FC scheme, and subsequently, to allow unmodified updraft air and condensate to detrain and mix throughout the grid element before evaporation is allowed. Although Fig. 17a suggests that the environment is warmed slightly by updraft detrainment at some levels, the concomitant evaporative cooling must be more than enough to offset this effect. The net thermal impact of updraft mass detrainment at any level must be negative.) Detrainment of relatively cool overshooting updraft air introduces a negative temperature tendency near cloud top. However, the intense heating–cooling couplet that is so prominent in the severe storm heating profile does not develop in this environment because (i) static stability is much lower near cloud top, reducing the subsidence warming effect, and (ii) updraft parcels carry less vertical momentum up to the equilibrium temperature level so that they lose their upward momentum and detrain before they become much colder than their environment.

Parameterized drying effects are also quite sensitive to cloud model type in this environment, as revealed by Fig. 15b. The ODEDP promotes much stronger drying in the lower troposphere than the other two

models, consistent with the subsidence profiles shown in Fig. 16a. Perhaps the more significant difference, however, occurs in the middle and upper troposphere. Figure 17b shows that detrainment of moisture simulated by the ODEDP strongly opposes subsidence drying at all levels above cloud base, resulting in a net moistening of the resolvable-scale environment above 650 mb.

This type of behavior by the ODEDP may have significant implications for numerical modeling of mesoscale convective systems. Observations and modeling studies suggest that a substantial fraction of the precipitation in these systems falls from clouds that are distinctly stratiform in character (e.g., see Gamache and Houze 1983; Hauser and Ameyenc 1986). These studies also suggest that detrainment from convective clouds represents an important source of moisture for the stratiform regions of these systems. Frank and Cohen (1987) found that a sufficiently large parameterized detrainment rate from convective clouds is critically important to the numerical simulation of tropical convective systems. It is offered that the ODEDP provides a physically realistic mechanism for parameterizing the moisture detrainment rate in any environment.

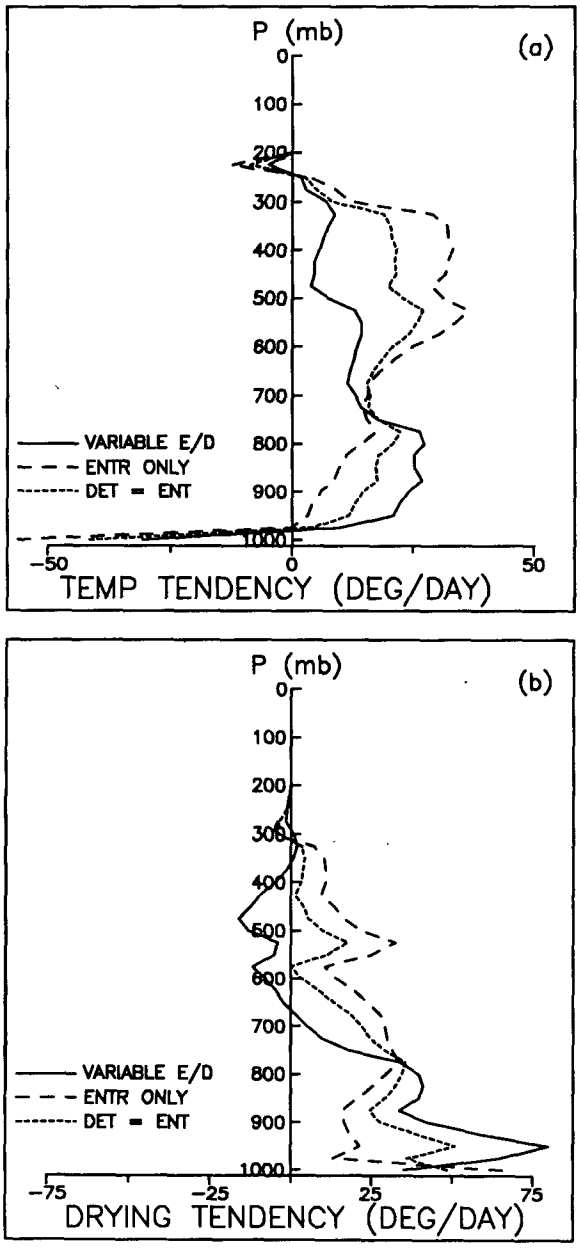

FIG. 15. Parameterized convective heating (a) and drying (b) profiles as a function of cloud-model type for the GATE composite sounding shown in Fig. 14.

d. Comparison with observations

Comparison of parameterized heating and drying profiles with diagnosed values involves considerable subjectivity because the time and space scales of the parameterized and observed effects are often highly disparate. Furthermore, diagnosed profiles usually reflect some (unknown) combination of convective and stratiform precipitation, whereas only deep convection is parameterized in the FC scheme. In spite of these limitations, the results of Frank and McBride (1989), who compared heating and drying profiles diagnosed in the GATE environment to those estimated from AMEX (Australian Monsoon Experiment) data, are encouraging. They found that both heating and drying tended to maximize considerably lower in the atmosphere during most stages of GATE convective systems than during comparable stages of AMEX systems. As noted by Frank and McBride, their AMEX composite sounding (Fig. 18) is characterized by a vertical temperature profile that is nearly parallel to that of the GATE composite. The primary difference between the two environments is the relatively dry midlevels in the GATE sounding. Their diagnosed heating profiles from the earliest stage of mesoscale convective systems are compared to those obtained using the ODEDP in the modified FC CPS with composite soundings from the same time period. It is assumed that this stage is most appropriate because the diagnosed heating profiles are likely to be less strongly influenced by stratiform precipitation than during the later stages.

Figure 19 shows the diagnosed heating profiles of Frank and McBride (1989) for each environment. The diagnosed vertical distribution of heating in the GATE environment coincides remarkably well with the present parameterized profile (Fig. 15a). The magnitudes are considerably different, but this is not surprising since the diagnosed profiles are derived from an observing network with a diameter of 800 km while the parameterized heating rates are based on a model grid element of 25 km. Figure 20 shows the parameterized heating profile obtained by initializing the present

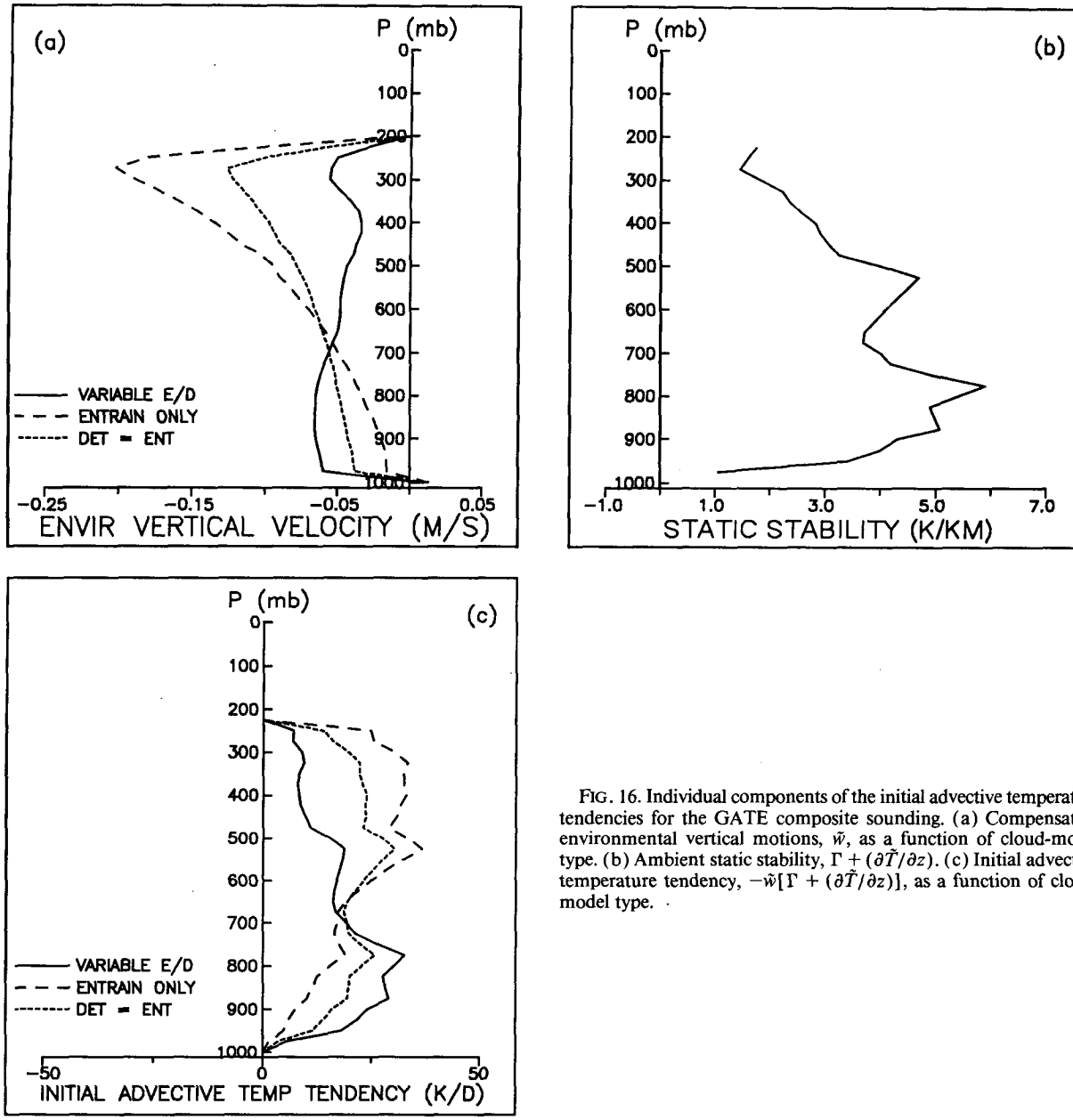

FIG. 16. Individual components of the initial advective temperature tendencies for the GATE composite sounding. (a) Compensating environmental vertical motions, $\tilde{w}$, as a function of cloud-model type. (b) Ambient static stability, $\Gamma + (\partial\tilde{T}/\partial z)$. (c) Initial advective temperature tendency, $-\tilde{w}[\Gamma + (\partial\tilde{T}/\partial z)]$, as a function of cloud-model type.

scheme with the AMEX sounding (assuming an updraft radius of 1 km). Once again, the vertical distribution agrees quite well with the diagnosed profile.

Since the thermal structures of these environments are so similar, there is some suggestion that the distinct differences in the heating distributions may be dictated by the dissimilar moisture profiles. The ability of ODEDP to reproduce the diverse heating distributions provides substantial evidence that the physical processes represented by the entrainment/detrainment scheme significantly influence the vertical distribution of heating and drying by convective clouds.

5. Discussion and summary

A modified version of the one-dimensional entraining plume model designed specifically to represent clouds in convective parameterization schemes has been introduced. The model is unique in its representation of mixing processes between clouds and their environments. In a manner conceptually similar to Raymond and Blyth (1986), a buoyancy sorting mechanism is allowed to partition mixtures containing various proportions of updraft and environmental air into entraining and detraining components of a two-

way mass exchange process across the interface of clear and cloudy air. Unlike the aforementioned authors, however, the present study avoids tracing the paths of individual cloud subparcels. Instead, integration over an assumed distribution of mass in the collective mixed subparcels yields the net entrainment and detrainment rates. The new model enhances the sensitivity of a convective parameterization scheme to the cloud scale environment primarily by (i) introducing a physically realistic mechanism for estimating the rate of lateral detrainment of cloud mass at any level and (ii) allowing the vertical profile of updraft mass flux to vary as a function of environmental conditions in the cloud layer.

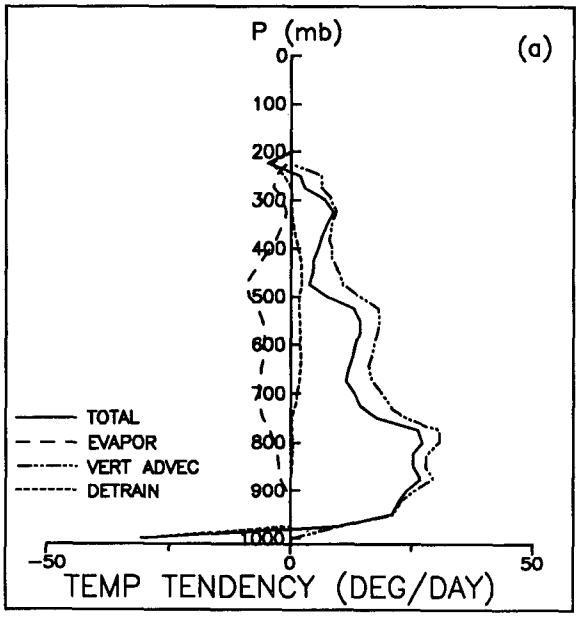

FIG. 17. Individual components of parameterized convective heating (a) and drying (b) for the GATE composite sounding when the ODEDP model is used.

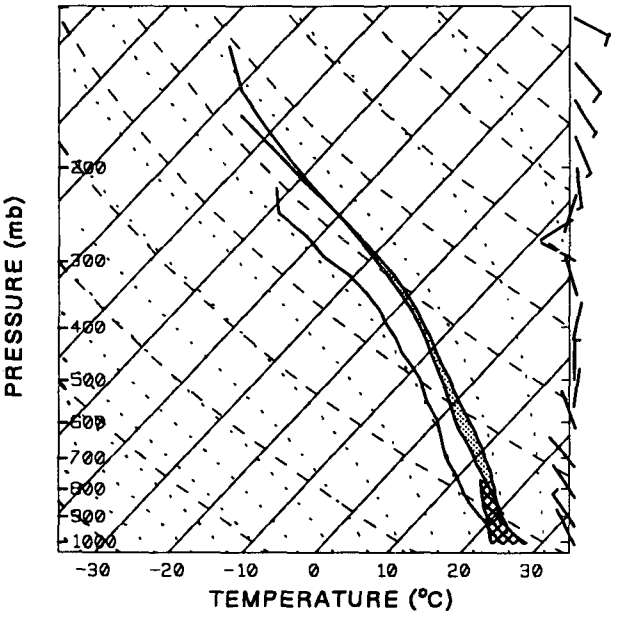

FIG. 18. AMEX composite environmental sounding showing the positive area given by the ODEDP cloud model (stippled) and the downdraft negative area given by the downdraft plume model in the modified FC scheme (cross-hatched).

The ODEDP is considerably more sophisticated than a plume model, that specifies a one-way exchange of mass across cloud boundaries, or one in which the detrainment rate is specified as a constant fraction of the entrainment rate. However, it still represents a gross simplification of the physical processes that occur in real convective clouds. Accordingly, its mathematical formulation necessitates rather arbitrary specification of some key parameters. The sensitivity of the mass flux profiles generated by the ODEDP to variations in a number of these parameters has been investigated.

Of particular concern to the integrity of the formulation is the specification of a frequency distribution of individual updraft subparcels as a function of mixing proportions. It is reasoned that there must be some preferred mode of mixing such that certain combinations of updraft and environmental air are preferred over others and a Gaussian-type distribution to characterize this process is imposed. Results indicate that the ODEDP mass flux profiles are relatively insensitive to variations about this distribution.

Additional sensitivity tests show that the rate at which environmental air mixes with the updraft has a strong influence on the mass flux profiles generated by the ODEDP. Of fundamental concern in this regard is

the ability to realistically estimate variations in environmental inflow as a function of resolvable scale forcing in a prognostic application. Since there is some indication that cloud size is related to the rate of localized mass convergence, an investigation of the possibility of specifying the rate of environmental inflow as a function of resolvable scale mass convergence when the ODEDP is used within a numerical weather prediction model is planned.

Most significantly, the sensitivity tests demonstrate that ODEDP mass flux profiles are most profoundly influenced by variations in cloud layer environmental conditions. This characteristic should allow a convective parameterization scheme to be much more responsive to various convective environments than it would be with a cloud model in which entrainment and detrainment rates are prespecified.

The efficacy of the ODEDP using the Fritsch–Chappell convective parameterization scheme was evaluated and it was found that parameterized heating and drying profiles are relatively insensitive to the type of cloud model used in a severe storm environment, but that they vary significantly as a function of cloud-model type in a tropical environment. Since the original Fritsch–Chappell scheme was developed on the basis of observations in continental midlatitude environments and its successful performance under these conditions has been documented (e.g., see Zhang and Fritsch 1986; Zhang and Gao 1989), these results are not surprising. It is anticipated that the ODEDP will render the modified FC scheme much more responsive to convective environments found in maritime tropical regions than the original scheme.

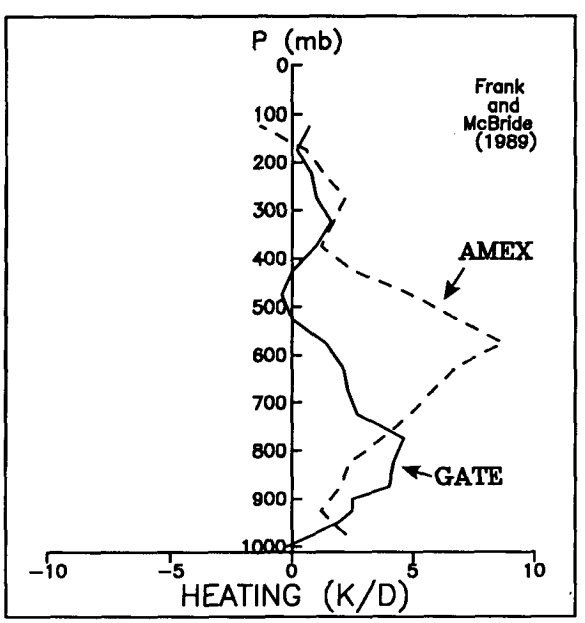

FIG. 19. Diagnosed vertical distributions of diabatic heating from Frank and McBride (1989) for the initial stages of mesoscale convective systems in the GATE and AMEX environments.

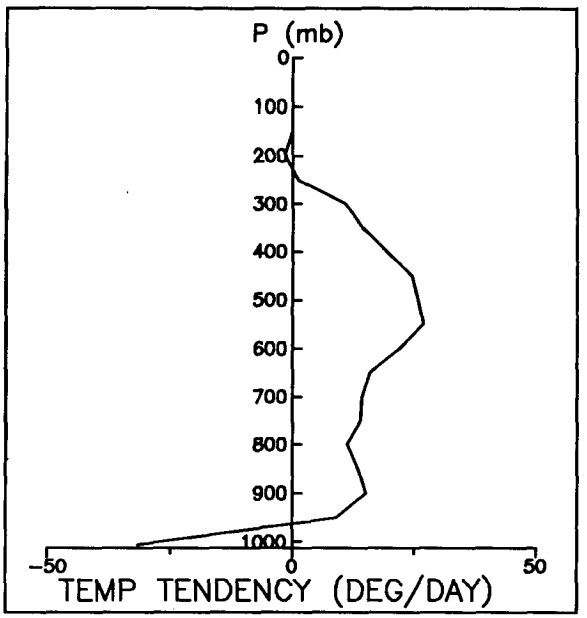

FIG. 20. Parameterized convective heating profile for the AMEX composite sounding derived using the ODEDP cloud model.

Through a detailed analysis of the individual components of parameterized heating and drying, the dominant contribution of subsidence effects have been quantified. However, the present results suggest that lateral detrainment effects may substantially offset, and even dominate, the effects of compensating subsidence in some environments. In particular, it appears that lateral detrainment from clouds has the greatest impact in marginally unstable and/or relatively dry convective environments.

The sensitivities inherent in the ODEDP render it valid only in a prognostic numerical model with horizontal resolution fine enough to resolve the environment of individual cumulonimbus clouds. It is suggested that this constraint imposes an upper limit on the horizontal grid length of ~30 km when the ODEDP is used. Accordingly, it is proposed that the characteristics and performance of this model present important considerations for convective parameterizations in the next generation of large-scale, operational numerical weather prediction models. Several mesoscale models are already being run on an operational basis (e.g., Gadd 1985; Warner and Seaman 1990), but typically over a limited regional domain. As the horizontal domain in mesoscale models is expanded, and as the horizontal resolution in larger-scale models approaches the scale of individual convective clouds, greater flexibility in these models' parameterization of subgrid scale convection will be necessary to represent disparate convective environments faithfully.

The present results suggest that an interactive entraining/detraining plume model may provide a critical component of the extra sensitivity that appears to be necessary for the universal application of convective parameterization schemes in larger-scale numerical models.

Acknowledgments. We thank Morris Weisman, Harry Orville, Michael Weissbluth and Bill Cotton for sharing data from their cloud-scale numerical modeling studies. We appreciate the many insightful discussions on cloud modeling and convective parameterization with Da-lin Zhang, Bill Frank and Charlie Cohen. Thanks are also extended to Nelson Seaman for his helpful suggestions on the contents of this manuscript. We are especially grateful for the thorough reviews and helpful suggestions of Dave Raymond and Brad Ferrier. This work was supported by National Science Foundation Grant ATM-87-11014 and Naval Research SFRC N00014-86-K-0688.

REFERENCES

Anthes, R. A., 1977: A cumulus parameterization scheme utilizing a one-dimensional cloud model *Mon. Wea. Rev.*, **105,** 270–286.

Arakawa, A., and W. H. Schubert, 1974: Interaction of a cumulus cloud ensemble with the large-scale environment, Part I. *J. Atmos. Sci.*, **31,** 674–701.

Blyth, A. M., W. A. Cooper and J. B. Jensen, 1988: A study of the source of entrained air in Montana cumuli. *J. Atmos. Sci.*, **45,** 3944–3964.

Bolton, D., 1980: The computation of equivalent potential temperature. *Mon. Wea. Rev.*, **108,** 1046–1053.

Cho, H.-R., 1975: Cumulus cloud population and its parameterization. *Pure Appl. Geophys.*, **113,** 837–849.

Frank, W. M., 1983: The cumulus parameterization problem. *Mon. Wea. Rev.*, **111,** 1859–1871.

——, and C. Cohen, 1985: Properties of tropical cloud ensembles estimated using a cloud model and an observed updraft population. *J. Atmos. Sci.*, **42,** 1911–1928.

——, and C. Cohen, 1987: Simulation of tropical convective systems. Part II: Simulations of moving cloud lines. *J. Atmos. Sci.* **44,** 3800–3820.

——, and J. L. McBride, 1989: The vertical distribution of heating in AMEX and GATE cloud clusters. *J. Atmos. Sci.*, **46,** 3464–3478.

Fritsch, J. M., 1986: Precipitation Enhancement—a scientific challenge. *Modification of mesoscale convective weather systems. Meteor. Monogr., No. 21,* Amer. Meteor. Soc., 77–86.

——, and C. F. Chappell, 1980: Numerical prediction of convectively driven mesoscale pressure systems. Part I: Convective parameterization. *J. Atmos. Sci.*, **37,** 1722–1733.

——, —— and L. R. Hoxit, 1976: The use of large-scale budgets for convective parameterization. *Mon. Wea. Rev.*, **104,** 1408–1418.

Gadd, A. J., 1985: The 15-level weather prediction model. *Meteor. Mag.*, **114,** 222–226.

Gamache, J. F., and Houze, R. A., 1983: Water budget of a mesoscale convective system in the tropics. *J. Atmos. Sci.*, **40,** 1835–1850.

Gardiner, B. A., and D. P. Rogers, 1987: On mixing processes in continental cumulus clouds. *J. Atmos. Sci.*, **44,** 250–259.

Gyakum, J. R., 1983: On the evolution of the *QE II* storm. II: Dynamic and thermodynamic structure. *Mon. Wea. Rev.*, **111,** 1156–1173.

Hack, J. J., and W. H. Schubert, 1986: Nonlinear response of atmospheric vortices to heating by organized cumulus convection. *J. Atmos. Sci.*, **43,** 1559–1573.

Hallett, J., R. I. Sax, D. Lamb and A. S. R. Murty, 1978: Aircraft measurements of ice in Florida cumuli. *Quart. J. Roy. Meteor. Soc.*, **104,** 631–651.

Hauser, D., and P. Ameyenc, 1986: Retrieval of cloud water and water vapor contents from doppler radar data in a tropical squall line. *J. Atmos. Sci.*, **43,** 823–838.

Heymsfield, A. J., and D. J. Musil, 1982: Case study of a hailstorm in Colorado. Part II: Particle growth processes at midlevels deduced from in-situ measurements. *J. Atmos Sci.*, **39,** 2847–2866.

Jensen, J. B., and A. M. Blyth, 1988: Comment on "Mixing mechanisms in cumulus congestus clouds. Part I: Observations". *J. Atmos. Sci.*, **45,** 2460–2463.

Johnson, R. H., 1977: The effects of cloud detrainment on the diagnosed properties of cumulus populations. *J. Atmos. Sci.*, **34,** 359–366.

Jorgensen, D. P., and M. A. LeMone, 1989: Vertical velocity characteristics of oceanic convection. *J. Atmos Sci.*, **46,** 621–640.

Kain, J. S., 1989: A one-dimensional entraining/detraining plume model and its application in convective parameterization. M.S. thesis, Pennsylvania State University. 143 pp. [Available from Dept. of Meteorology, 503 Walker Building, University Park, PA 16802.]

Knupp, K. R., and W. R. Cotton, 1985: Convective downdraft structure: An interpretive survey. *Rev. Geophys.*, **23,** 183–215.

Kreitzberg, C. W., and D. J. Perkey, 1976: Release of potential instability. Part I: A sequential plume model within a hydrostatic primitive equation model. *J. Atmos. Sci.*, **33,** 456–475.

Krueger, S. K., 1988: Numerical simulation of tropical cumulus clouds and their interaction with the subcloud layer. *J. Atmos. Sci.*, **45,** 2221–2250.

Kuo, H. L., 1974: Further studies of the parameterization of the influence cumulus convection on large scale flow. *J. Atmos. Sci.*, **31,** 1232–1240.

Kuo, Y.-H., and R. J. Reed, 1988: Numerical simulation of an explosively deepening cyclone in the eastern Pacific. *Mon. Wea. Rev.*, **116,** 2082–2105.

LeMone, M. A., and E. J. Zipser, 1980: Cumuloniumbus vertical velocity events in GATE. Part I: Diameter, intensity, and mass flux. *J. Atmos. Sci.*, **37,** 2444–2457.

Lord, S. J., 1982: Interaction of a cumulus cloud ensemble with the large-scale environment. Part III: Semiprognostic test of the Arakawa-Schubert cumulus parameterization. *J. Atmos. Sci.*, **39,** 88–103.

——, H. E. Willoughby, and J. M. Piotrowicz, 1984: Role of a parameterized ice-phase microphysics in an axisymmetric, nonhydrostatic tropical cyclone model. *J. Atmos. Sci.*, **41,** 2836–2848.

Ogura, Y., and H.-R. Cho, 1973: Diagnostic determination of cumulus cloud populations from observed large-scale variables. *J. Atmos. Sci.*, **30,** 1276–1286.

Ooyama, K., 1971: A theory on parameterization of cumulus convection. *J. Meteorol. Soc. Jpn.* **49,** 744–756.

Paluch, I.R., and C. A. Knight, 1984: Mixing and the evolution of cloud droplet size spectra in a vigorous continental cumulus. *J. Atmos. Sci.*, **41,** 1801–1815.

——, and D. G. Baumgardner, 1989: Entrainment and fine scale mixing in a continental convective cloud. *J. Atmos. Sci.*, **46,** 261–278.

Raymond, D. J., and A. M. Blyth, 1986: A stochastic mixing model for nonprecipitating cumulus clouds. *J. Atmos Sci.*, **43,** 2708–2718.

Rogers, D. P., J. W. Telford and S. K. Chai, 1985: Entrainment and development of the microphysics of convective clouds. *J. Atmos. Sci.*, **42,** 1846–1858.

Simpson, J., 1971: On cumulus entrainment and one-dimensional models. *J. Atmos. Sci.*, **28,** 449–455.

——, 1983: Cumulus clouds: interactions between laboratory experiments and observations as foundations for models. *Mesoscale Meteorology,* D. K. Lilly and T. Gal-Chen, Eds., Reidel, 399–412.

——, and V. Wiggert, 1969: Models of precipitating cumulus towers. *Mon. Wea. Rev.*, **97**, 471–489.

Tao, W.-K., and J. Simpson, 1984: Cloud interactions and merging: numerical simulations. *J. Atmos. Sci.*, **41**, 2901–2917.

——, ——, and M. McCumber, 1989: An ice-water saturation adjustment. *Mon. Wea. Rev.*, **117**, 231–235.

Turner, J. S., 1962: The starting plume in neutral surroundings. *J. Fluid Mech.*, **13**, 356–368.

Waldvogel, A., L. Klein, D. J. Musil and P. L. Smith, 1987: Characteristics of radar-identified big drop zones in Swiss hailstorms. *J. Climate Appl. Meteor.*, **26**, 861–877.

Warner, T. T., and N. L. Seaman, 1990: A real-time, mesoscale numerical weather prediction system used for research, teaching, and public service at The Pennsylvania State University. *Bull. Amer. Meteor. Soc.*, **71**, 792–805.

Yanai, M., S. Esbensen and J.-H. Chu, 1973: Determination of bulk properties of tropical cloud clusters from large-scale heat and moisture budgets. *J. Atmos. Sci.*, **30**, 611–627.

Zhang, D.-L., 1989: The effect of parameterized ice microphysics on the simulation of vortex circulation with a mesoscale hydrostatic model. *Tellus*, **41A**, 132–147.

——, and J. M. Fritsch, 1986: Numerical simulation of the meso-β scale structure and evolution of the 1977 Johnstown flood. Part I: Model description and verification. *J. Atmos. Sci.*, **43**, 1913–1943.

——, and K. Gao, 1989: Numerical simulation of an intense squall line during 10–11 June 1985 PRE-STORM. Part II: Rear inflow, surface pressure perturbations, and stratiform precipitation. *Mon. Wea. Rev.*, **117**, 2067–2094.